POLITECNICO
MILANO 1863

DIPARTIMENTO DI MECCANICA

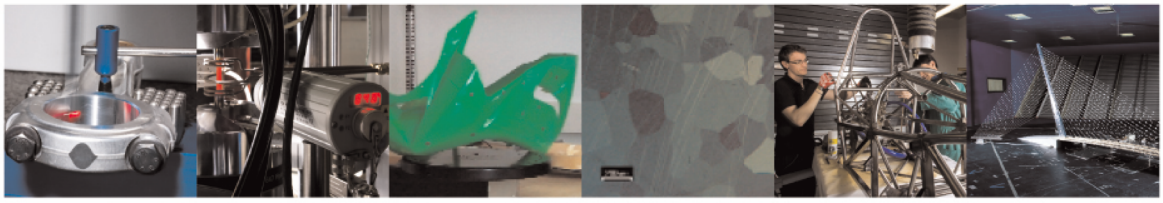

Ball-milled Al-Sn alloy as composite Phase Change Material

Chiara Confalonieri, Aldo Tommaso Grimaldi, Elisabetta Gariboldi

This is a post-peer-review, pre-copyedit version of an article published in Materials Today Energy. The final authenticated version is available online at:
http://dx.doi.org/10.1016/j.mtener.2020.100456

Ball-milled Al-Sn alloy as composite Phase Change Material

Chiara Confalonieri[a]*, Aldo Tommaso Grimaldi[a,1], Elisabetta Gariboldi[a]

[a]Politecnico di Milano, Department of Mechanical Engineering, Via La Masa 1, 20156 Milan (Italy)

chiara.confalonieri@polimi.it, aldo.tommaso.grimaldi@mi.infn.it, elisabetta.gariboldi@polimi.it

*corresponding author

Abstract

The present study concerns a fully metallic solid-liquid composite Phase Change Material based on an Al-Sn Miscibility Gap Alloy produced by powder metallurgy, including its ball-milling, compression and further sintering heat treatment. The materials obtained by different routes display a narrow melting temperature range at about 230°C, corresponding to the phase transformation of Sn- or of Sn-rich eutectic. The microstructures obtained by this manufacturing process lead to form-stable PCMs, which can keep their shape and prevent active phase leakage in service conditions. Ball milling of metal powders as mixing technique allowed to obtain a very fine microstructure, resulting in stability of thermal response and improvement of mechanical properties. Among the investigated Al-40Sn mass% samples, the most promising were those compressed at 240°C followed by sintering at 500°C.

Keywords: metallic Phase Change Materials; form-stable; ball milling; thermal stability; microstructure.

1. Introduction

Phase Change Materials (PCMs) are materials in which a phase transition occurs under specific conditions and causes a significant change in at least one material property. Considering thermal properties, they can be applied as Thermal Energy Storage (TES)

[1] Present address: Istituto Nazionale di Fisica Nucleare (INFN) – Laboratorio Acceleratori e Superconduttività Applicata (LASA), Via Fratelli Cervi 201, 20090 Segrate (Milan, Italy)

systems, storing the latent heat associated to the phase transition. This approach is referred as latent heat storage (LH TES) and Kuta et al. [1] consider it as the most efficient way to store thermal energy; in facts, according to Fiedler et al. [2], this approach allows to store a higher energy density using less material. PCMs can be applied in several different fields. Kuta et al. [1] reported PCM-based building envelopes, which can keep proper internal conditions storing or releasing energy depending on external conditions, thus reducing the use of air conditioning or heating. Navarrete et al. [3] proposed to use self-nanoencapsulated metal/metal alloys to enhance thermal property of a Heat Transfer Fluid, obtaining a nanofluid. Considering solar energy sector, Reed at al. [4] developed a C-(Al-Si) system to be applied in concentrated solar power plants. In addition, Nazir et al. [5] reviewed many other applications, like thermal management in photovoltaic cells, smart textiles and cooling systems in electronic devices.

According to Sun et al. [6], the most important properties of PCMs for TES are the transition temperature and the latent heat associated to the transition; at the same time, good thermal stability and reliability of thermal performance. Moreover, Wei et al. [7] mentioned as desired properties also high thermal conductivity, high specific heat and high density. For some applications, also good mechanical properties could be required. Although every phase transition (gas-liquid, solid-gas, solid-liquid, solid-solid) could be exploited to store energy, usually only solid-solid and solid-liquid transition are applied, due to the large volume changes associated to gas transitions. Among them, solid-liquid transitions have generally higher latent heat with respect to solid-solid ones; however, the liquid phase needs to be enclosed in some way to avoid leakage. The main properties of potential PCMs based on solid-liquid transition are shown in Table 1. Among the wide range of materials that have been considered as PCMs for TES and, more in general, for thermal management of systems, metallic PCMs are so far the less developed class; Mohamed et al. [8] ascribed this fact to their low heat of fusion per unit weight.

Nevertheless, as highlighted by Zhou and Wu [9], they have higher operative temperature ranges (including phase transition) which makes them suitable for high-temperature applications. Moreover, they have higher latent heat per unit volume, which makes them attractive for compact devices.

Active Phase	PCM type	Transition temperature	Density	Latent heat		Reference
				per unit mass	per unit volume	
		°C	g/cm^3	J/g	J/cm^3	
Paraffin ($C_{29}H_{60}$)	organic	63,4	0,81	239	193	[10]
$MgCl_2$•$6H_2O$	inorganic	117	1,57	167	262	[11]
Sn	metallic	232	7,29	59	430	[12]
Cu	metallic	1085	8,93	205	1831	[12]

Table 1. Main properties of some potential solid-liquid PCMs

In addition to the 'classic' goals of maximizing thermal response and stability, the design of metallic PCM can be based on the possibility to exploiting the structural properties typical of metals. Metallic solid-liquid PCMs are usually produced by encapsulation of the active phase in a passive-phase capsule, whose size ranges from millimetres to nanometres. However, Zhou and Wu[9] highlighted that encapsulated PCMs may oxidize or deteriorate particularly at high temperatures, reducing durability and energy storage performance; moreover, Pielichowska and Pielichowski [13] observed that encapsulation process can be complex and expensive.

To overcome these issues, Zhou and Wu [9] suggest to use of solid-solid PCMs. Another viable alternative is the choice of alloys which behave as form-stable PCMs (FS-PCMs), i.e. materials in which the active phase (the actual PCM) is embedded in a higher-melting passive matrix, which remains solid at all stages preventing leakage and keeping structural properties, as defined by Pielichowska and Pielichowski [13]. According to Sugo et al. [14], thermal energy storage at high temperature is most efficient and compact using two-phase mixtures in which phases are completely immiscible at solid state: in this way, it is possible to prevent the formation of solid solutions or intermetallics, keeping the composition of the

two phases stable over time or with thermal cycles. So, Sugo et al. [14] suggested that alloys with these features can be obtained exploiting miscibility gaps in phase diagrams and so they are called Miscibility Gap Alloys (MGAs); examples of MGAs are Al-Sn, Fe-Cu and Fe-Mg alloys. Among them, Sugo et al. [14] recommended Al-Sn based alloys as one of the metallic systems to be applied as PCMs for high temperature energy storage, characterized by activation temperatures close to 230°C (232°C for pure Sn).

Al-Sn based alloys are often used as bearing alloys, thanks to their excellent tribological properties; the target microstructure for this application [15] is similar to the one desired for metallic PCMs. A previous study on PCMs by Gariboldi and Perrin [16] focused on an Al alloy with 20% volume content of Sn, which corresponds to about 40% mass content; the same alloy composition was considered in this paper, as shown on the Al-Sn phase diagram in Figure 1. This Sn content is higher than in bearing alloys, which is usually lower than 30 mass%; for example, Liu et al. [15] used 20% mass of Sn and Noskova et al. [17] used 30% mass. The goal of the study was to verify if it is possible to use well-known and proven industrial processes for bearing alloys also to produce FS-PCMs.

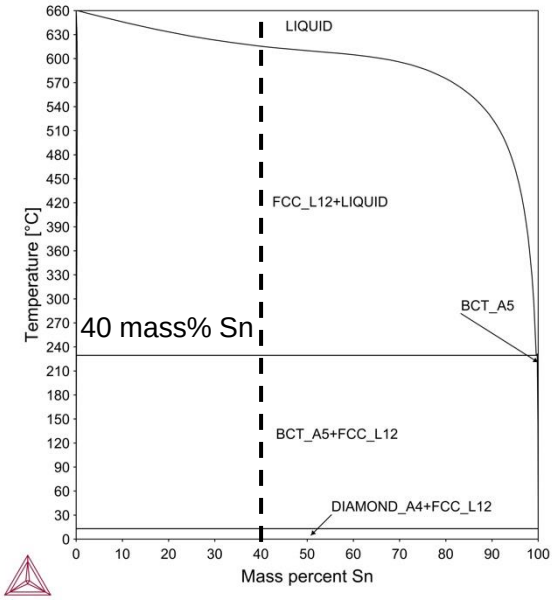

Figure 1. Al-Sn phase diagram with considered composition (computed using Thermo-Calc Software TCAL6 Aluminium-based alloys database, accessed 9 January 2019)

In practice, it is not so trivial to obtain the target microstructure, since natural cooling results in an opposite structure (matrix surrounded by active-phase particles). Among the possible solutions listed by Liu et al. [18], powder metallurgy is a group of manufacturing techniques which allows to obtain MGAs with “inverse microstructure”. The process involves mixing, compression and finally sintering of powders; in this way, the matrix material can form a continuous body which completely encapsulates the active phase, preventing leakage in operative conditions. As a matter of fact, the resultant morphology of the active phase depends on the initial shape and size distribution of the powdered components, as well as on process parameters. In the abovementioned previous study by the research group [16], relatively fine Sn powders were simply mixed. Ball milling (BM) is the most common comminution technique to obtain fine particles from solids and it is often used in the production of bearing alloys. When a mixture of metal powders is subjected to ball milling, powder particles are mixed and reduced in size at the same time, resulting in a homogeneous alloy; therefore, the whole process is called Mechanical Alloying [19]. The expected difference between simple mixed and ball milled microstructures was a finer structure. Nonetheless, ball milling is more complex and expensive than simple mixing process. A preliminary check on ball-milling production route by Confalonieri et al. [20] suggested promising microstructures, independently on the size-distribution of Sn powders adopted. The innovative feature of the research presented in this paper is the insertion of ball milling of Sn powders into an overall production cycle to obtain FS-PCMs. Compression as well as sintering temperatures were selected as parameters of these process stages. Their effect on microstructures, thermal response and mechanical properties of the FS-PCMs was investigated before and after simulated service, to check the material properties stability.

2. Materials and experimental procedures

Two Sn powders and an Al powder were selected for the present investigation. The Al powder was an atomized high purity Al (> 99.7 mass%) powder with diameters smaller than 45 μm (ECKA Granules GmbH, Germany). The two types of Sn powders (Metalpolveri S.r.l) having different particle size and distribution were considered: powder SN (Sn > 99.9 mass%), characterized by very fine particle-size distribution and good homogeneity, and powder 106 (Sn > 99.7 mass%), characterized by coarser particles with lower homogeneity. The second one has both a relatively high amount of fine particles (< 20 μm) and coarse particles (anyway, generally smaller than 100 μm). Either powder SN or powder 106 was mixed to Al powder to get nominal volumetric composition of the alloy equal to 80% Al and 20% Sn (corresponding to about 40 mass% Sn, as shown in Figure 1).

Each Al/Sn mixed powder was ball-milled using a planetary mill (Retsch PM 400 Planetary Ball Mill), which consists of four grinding jars that are arranged eccentrically on a sun wheel and rotate in the opposite direction with respect to it (speed ratio 1:2.5). Each Al-Sn mixed powder was sealed in stainless steel jar together with hardened steel balls (diameter 20 mm) in a ratio of 1:5 in order to have at least about 33% of empty space in the jar to assure an effective mixing. Ethanol was added as lubricant (4% on the total weight of powders) in order to avoid cold fusion phenomena. Protection from oxidation was achieved using a pure Ar atmosphere. Grinding process was conducted for 24 hours at 250 rpm; to avoid excessive increases in temperature due to friction and to further minimize oxidation phenomena, grinding cycles of 20 minutes were alternated to pause cycles of 10 minutes.

Then, ball-milled powders were compressed into cylindrical samples and sintered following the same parameters and procedures applied in the previous research on simple mixed powders [16]. Conversely to the case of bearing alloys, in which samples are usually

compressed at room temperature (i.e. cold compression, technique that had been checked by Confalonieri et al. [20]), compression was conducted at relatively high temperature (hot compression, HC), just below and above Sn melting temperature (about 232°C), i.e. at 220°C (HC220) and 240°C (HC240). In both cases, about 23 g of ball-mixed powders were compressed using an Instron 1195 Universal Testing Machine equipped with an extrusion set consisting of a hollow cylinder steel die and a 15 mm diameter punch; the die temperature was controlled by means of an induction heater (AHD Millennium 3-120-100 Inductor Heat Generator) whose coils surrounded the die. To assure a good densification, compression was divided into three steps: pre-compression up to 20 kPa, compression up to maximum pressure, i.e. 340 MPa, and, after a pause of 60 s to allow relaxation of the structure, final compression up to maximum pressure. In this way, samples with diameter of 15 mm and height of about 18 mm were obtained. Concerning heat treatments, fractions of the samples were sintered for 1 hour in pure Ar atmosphere at 250°C, which is a usual temperature for bearing alloys, or at 500°C, as proposed for PCMs by Sugo et al. [14]. At the end of the heat treatment, samples were slowly cooled down to room temperature in the furnace, keeping the Ar atmosphere. Then, to simulate service the samples were subjected to 100 thermal cycles in air at 20°C/min between 175°C and 285°C, thus including the melting/solidification temperature range of the active phase.

The material characterization in different manufacturing, heat treatment or simulated service conditions included microstructural, thermal and mechanical features. X-ray diffraction (XRD) analysis was carried out at room temperature using Panalytical X'Pert PRO MPD X-ray diffractometer (θ-θ geometry, Cu K_α source) to check crystallographic phases present after ball-milling. Microstructural characterization was carried out by Optical Microscopy (OM, Nikon Eclipse LV150NL) and Scanning Electron Microscopy (SEM, Zeiss EVO 50), after sample mounting and polishing. SEM micrographs were mainly taken detecting Backscattered Electrons (BSE), which highlight presence and

shape of Al and Sn phases thanks to their Z-contrast. In addition, Energy Dispersive Spectrometry (EDS) was used to check composition pointwise. analysis According to Underwood[21], if the volume fraction of porosity is assumed equal to its area fraction, the mean value of the porosity measured on 5 OM images at 100x magnification, each having area of about 1.2 mm^2, was considered; for this purpose, ImageJ open source software[22] was used. As far as the thermal characterization of PCM is concerned, Differential Scanning Calorimetry (DSC) analyses were performed to evaluate energy stored and released during thermal cycles, as usually done for PCMs. DSC tests were conducted on 55 mg samples obtained from central regions of cylinders in different processing conditions and after simulated service, using Setaram TG/DSC Labsys 1600. DSC test cycle consisted in heating at 20°C/min with a holding time of 5 min at 320°C, cooling at 20°C/min to 40°C, 5 min holding, the cycle being repeated. Finally, mechanical properties were evaluated by Vickers microhardness tests with load of 4.9 N and dwell time of 15 s, using Future-tech FM-700 microhardness tester.

3. Results

3.1 Microstructure

SEM-BSE images of samples obtained using the same process conditions, i.e. compression at 220°C, but containing different Sn-powder type (106 or SN) are shown in Figure 3. At low magnification, both samples show coarse homogeneous Sn particles ranging from a few microns to about 20 µm (bright), coarse Al-rich particles (darker) and regions of intermediate colour; in high magnification micrographs (Figure 3), the intermediate regions can be resolved as nanometric particles of Sn and Al. Stationary EDS analysis in relevant points confirmed the phase compositions inferred from SEM-BSE micrographs. A representative area where stationary EDS analysis was conducted is shown in Figure 2 and the relative results are reported in Table 2.

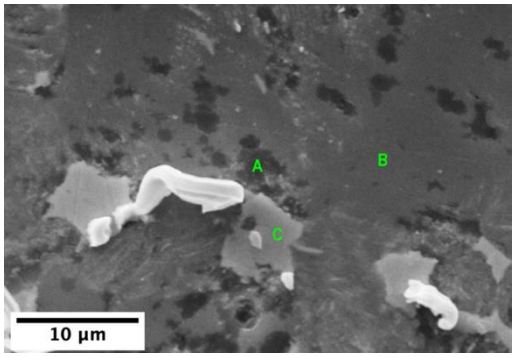

Figure 2. SEM micrograph of an area (sample HC220) where stationary EDS analysis was conducted in points A, B and C to measure phase composition.

Point	Element (mass%)			
	C	O	Al	Sn
A	8.51	14.60	66.25	10.64
B	12.30	3.81	79.82	4.07
C	2.80	0.30	0.90	96.00

Table 2. Results of stationary EDS analysis in points A, B and C of the area shown in Figure 2

In the sample HC220 produced with SN powder (Figure 3b), the presence of bright hair-like structures is observed; their thickness is a few microns, while their length ranges between 10 µm and a few hundreds of microns. They are identified as Sn whiskers, which formed after sample preparation for micrographic analysis. Although in minor quantity, they can be found also in other samples, despite the Sn powder type and the compression temperature; they seem to be absent in sintered samples. Samples obtained from 106-type Sn powders have just slightly coarser Sn-particles, but most of the remaining microstructural features are close to those of samples produced by SN powders. The limited effect of Sn powders selected to produce Al-Sn PCM via ball-milling, previously noticed in cold compressed samples [20], is here confirmed and is also reflected in close thermal and mechanical response. Therefore, samples produced with both powders will be here alternatively displayed and quantitative test results were averaged.

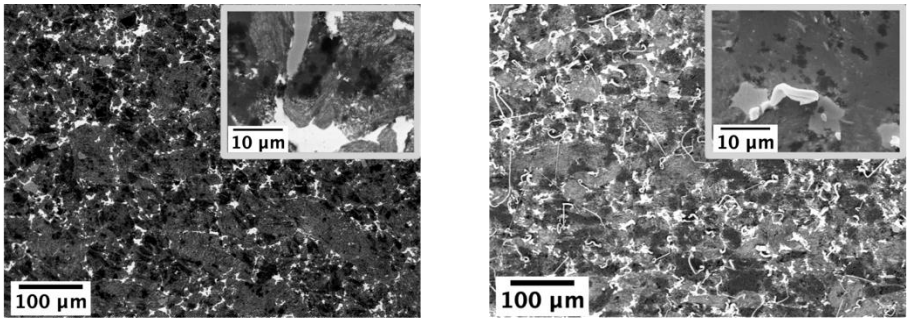

a) b)

Figure 3. SEM-BSE micrographs of samples compressed at 220°C using different Sn-powder types (106 for a and SN for b). Compression direction during compaction process: vertical. Higher magnification micrographs are shown in boxes at top right corner of each image

Some representative microstructures of the samples compressed at 240°C, as-compacted and after sintering at 250°C and 500°C, are presented in Figure 4.

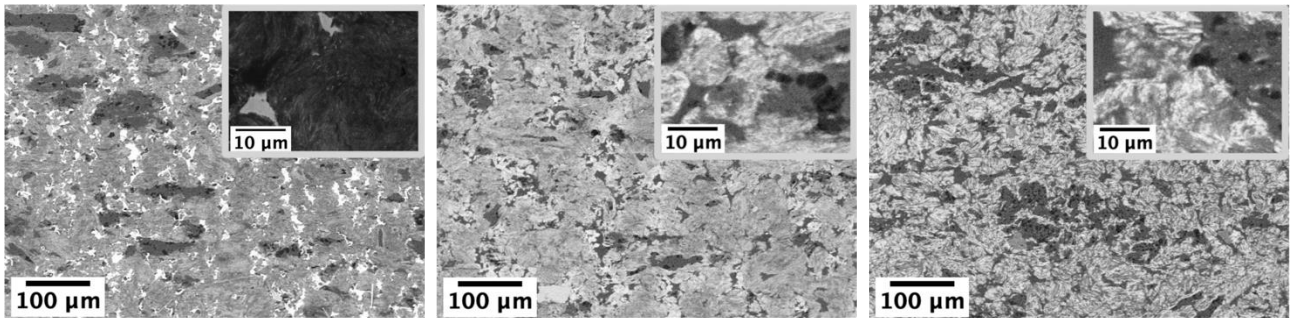

a) b) c)

Figure 4. SEM-BSE micrographs of samples compressed at 240°C and possibly sintered for 1 hour at different temperatures; from left to right, no sintering (a), sintering at 250°C (b), sintering at 500°C (c). Compression direction during compaction process: vertical. Higher magnification micrographs are shown in boxes at top right corner of each image

The same microstructural features observed in HC220 sample are present in the HC240 samples. However, it can be noticed that after sintering (Figure 4, b and c) there are no more micrometric homogeneous Sn particles and Sn is present only as nanometric particles in the in the light grey zone. From a visual analysis of sample surfaces at the end of production process, it was observed that no leakage occurred during hot compression, while a little leakage occurred during sintering.

After 100 thermal cycles carried out between 175 and 285°C to simulate service, visual analysis of sample surfaces revealed that leakage of Sn occurred for not-sintered samples, while sintered samples had no further Sn losses. Microstructural changes occurred in the above materials during simulated service can be appreciated comparing

the previous microstructures to those presented in Figure 5 and Figure 6, taken at the same magnification and with vertical compression direction during densification.

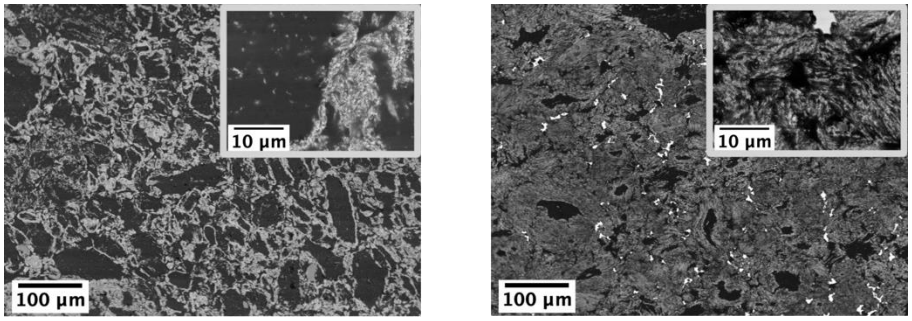

a) b)

Figure 5. SEM-BSE micrographs of not-sintered samples, after 100 cycles; from left to right, HC220 (a) and HC240 (b). Compression direction during compaction process: vertical. Higher magnification micrographs are shown in boxes at top right corner of each image

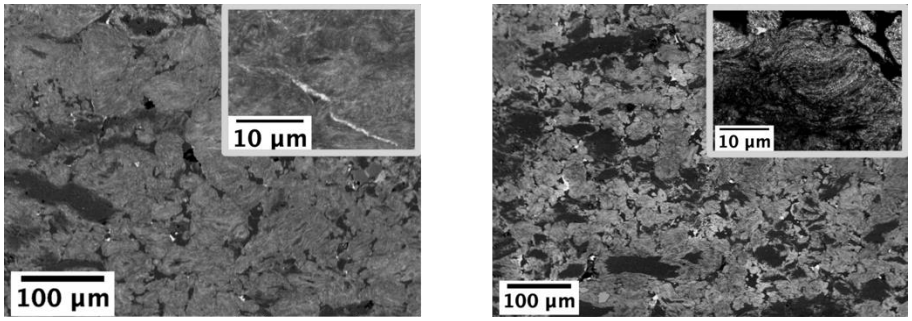

a) b)

Figure 6. SEM-BSE micrographs of samples compressed at 240°C and sintered, after 100 cycles. From left to right, sintering at 250°C and at 500°C for 1 hour. Compression direction during compaction process: vertical. Higher magnification micrographs are shown in boxes at top right corner of each image

The microstructure evolution involves the reduction of pure Sn coarse particles and the increase of the intermediate grey region consisting of nanometric particles of Sn and Al. These last features can be better observed in high-magnification micrograph in Figure 7; the microstructure is so fine that using Scanning Electron Microscopy is not possible to focus these small particles.

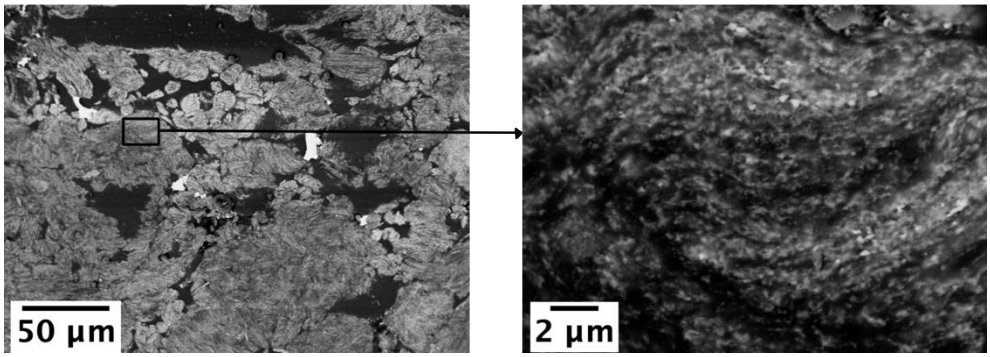

Figure 7. SEM-BSE image of Sn-rich region in sample compressed at 240°C and sintered at 500°C, after 100 cycles

The measured porosity area fractions for different process conditions is summarized in Figure 8. A generally high data scattering can be observed. This is due to difficulties in the evaluation (either automatic and manual) of porosities in such fine 2-phase microstructures which displays, both in OM and SEM micrographs, a darker phase (Sn using OM and Al using SEM) with features close to the small discontinuities. Therefore, a clear trend of porosity evolution with thermal treatments and thermal cycles could not be identified.

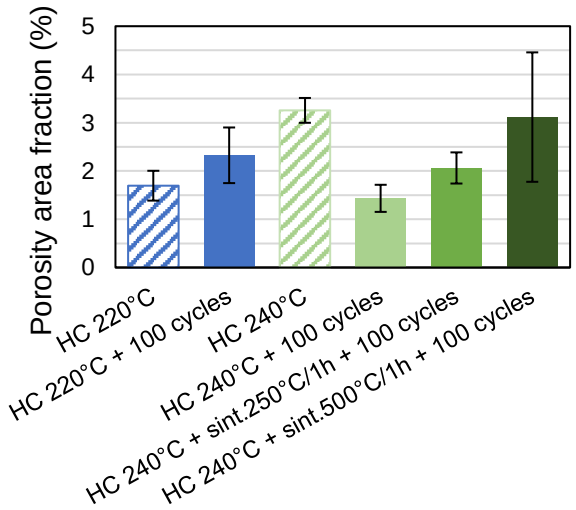

Figure 8. Porosity area fraction (%) for different process conditions

3.2 XRD analysis

The XRD analysis was carried out on as milled powders as well as on HC samples obtained from BM Al+SN powders compressed below and above Sn melting temperature (at 220°C and 240°C) to check which phases were present. Concerning HC samples, the test was conducted on a section parallel to compression direction in the middle of the sample with the same orientation. The results (Figure 9) demonstrate that there are no

other phases in addition to pure Al and pure β-Sn, neither in mixed powders nor in HC samples. Moreover, after hot compression, peaks do not show significant broadening with respect to powders. On the other hand, changes in peak intensities are observed in the different conditions, especially for tall peaks at low angle and for β-Sn phase.

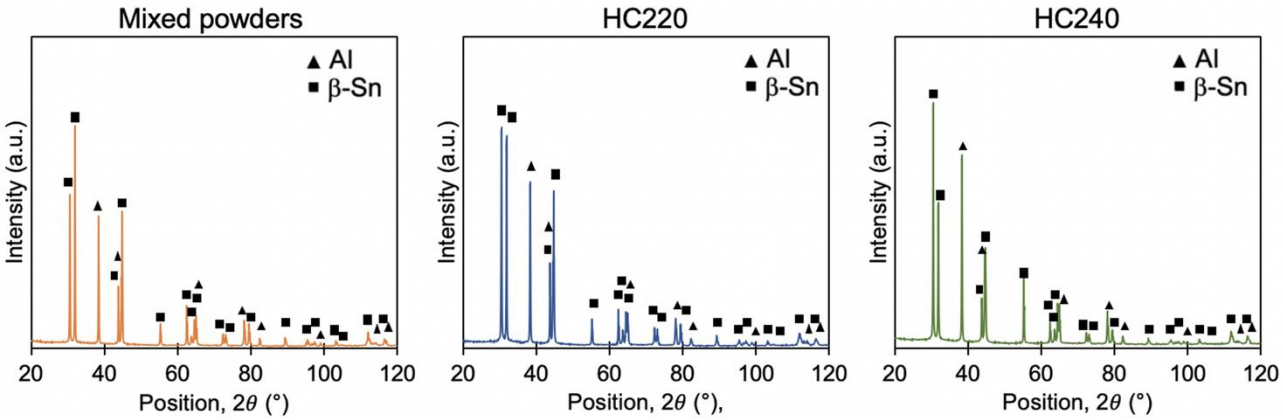

Figure 9. X-ray diffractogram of mixed powders, HC220 and HC240 samples in the as-compacted condition

3.3 Differential Scanning Calorimetry

The results of DSC tests, presented both in terms of heat flow vs. temperature curves and of enthalpies of melting and solidification, are summarized in Figure 10, Figure 11 and Table 3 for samples tested before and after thermal cycles simulating service.

Compression	*Sintering*	*100 cycles*	*Measured enthalpy (J/g)*		*Transition onset temperature (°C)*		*Transition peak temperature (°C)*	
			Melting	*Solidification*	*Melting*	*Solidification*	*Melting*	*Solidification*
HC220	-	-	40.20	-41.91	150.56	221.07	235.42	213.72
HC220	-	yes	23.84	-24.04	183.38	223.56	233.34	217.93
HC240	-	-	34.17	-33.16	157.56	221.98	233.52	212.04
HC240	-	yes	20.15	-21.07	160.05	224.94	233.12	178.17
HC240	250°C/1h	yes	18.76	-19.11	164.01	218.22	235.70	193.48
HC240	500°C/1h	yes	24.77	-26.58	154.33	220.00	230.99	208.42

Table 3. Measured enthalpy and transition temperature of all the tested samples in as-produced conditions and after thermal cycles simulating service

In Figure 10a, the comparison is between different compaction conditions: HC220 and HC240. Before thermal cycles, sample HC220, compacted just below the melting temperature of pure Sn and the eutectic Al-Sn temperature, displayed a clear single peak both in melting and in solidification, with an undercooling of at least 10°C for the latter. For

the specimen HC240, compacted above the melting temperature of pure Sn, only slight difference in melting peak is observed, while the solidification peak extends and broadens toward low temperatures. The broadening toward low temperatures as well as the presence of multiple thermal events in solidification characterize the above samples after thermal cycles simulating service, where maximum temperature reached is 285°C. Figure 10b summarizes the melting/solidification enthalpy derived from DSC curves in Figure 10a. Notwithstanding the different shape of peaks in melting/solidification, for each sample the corresponding enthalpy are almost the same. Moreover, a reduction of transition enthalpy with respect to the as-compacted samples is observed for all conditions after thermal cycles.

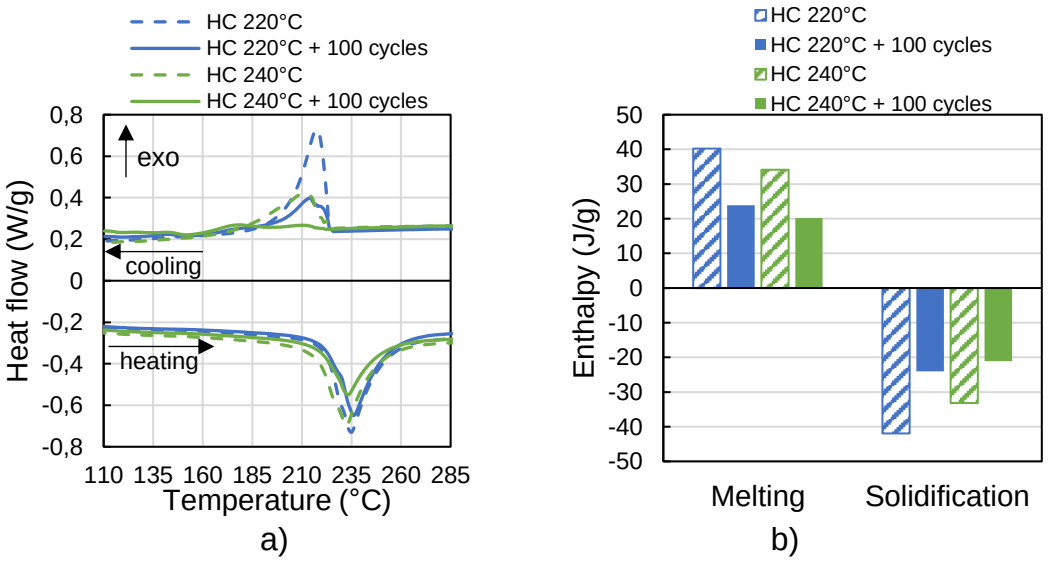

Figure 10. DSC curves (a) and specific enthalpy values (b) for samples produced in different compression conditions (HC220, HC240), before and after thermal treatment and cycles. The specific enthalpy values are the mean values of the results obtained for the two Sn-powder types.

Figure 11 focuses on the effect of sintering temperature and thermal cycling on samples compacted at 240°C. Figure 11a shows that the presence of broad and/or multiple solidification peaks is still observed after 100 cycles simulating service and the shape of thermal events still depends on the sintering condition. Figure 11b once again shows that, also in this set of samples, the enthalpy in melting and solidification corresponds for each sample. Further, it is clear that the sample sintered at 500°C kept relatively high enthalpy after simulated service, compared to the as-compacted sample.

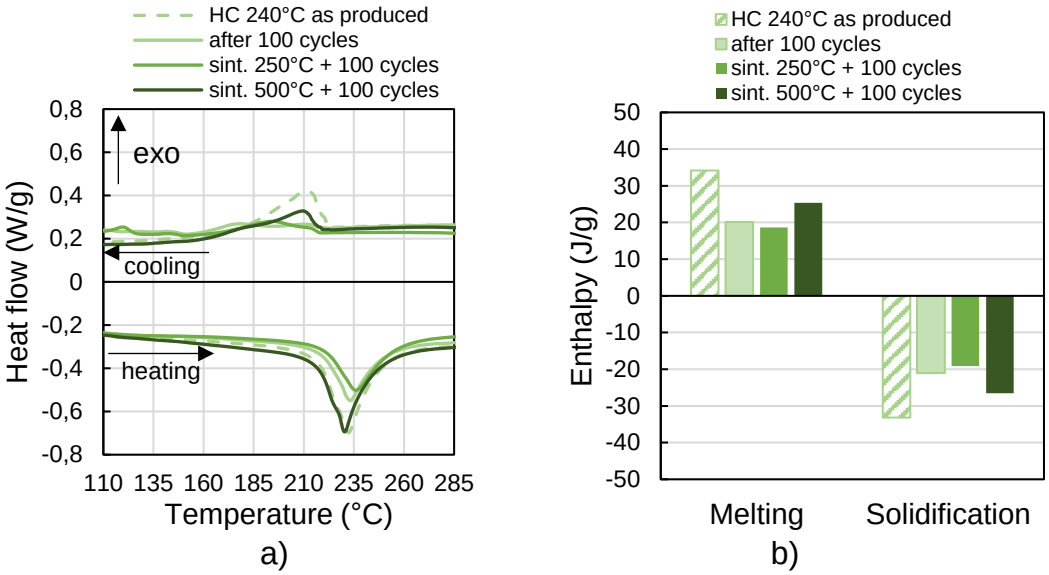

Figure 11. DSC curves (a) and specific enthalpy values(b) for sample produced by HC240 and possibly sintered at 250°C and 500°C, before and after thermal treatment and cycles. The specific enthalpy values are the mean values of the results obtained for the two Sn-powder types.

3.4 Mechanical behaviour

Vickers hardness results for samples in different as-compacted conditions are presented in Figure 12. Generally, simulated service only slightly reduced the hardness of all as-compacted samples. The effect of heat treatment is presented in Figure 13 for the representative case of the PCM compacted at 240°C; sintering at 500°C slightly reduced the mechanical response of the PCM, but the hardness of the sample sintered at this temperature is stable after simulated service. On the contrary, sintering at 250°C slightly increases hardness, but this reduced after simulated service.

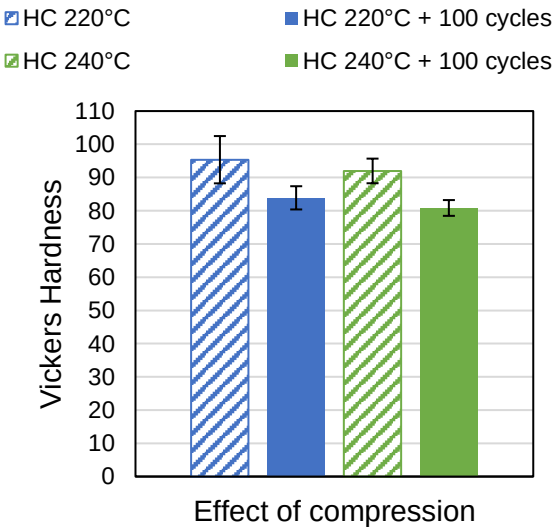

Figure 12. Vickers hardness values for samples produced in different compression conditions (CC, HC220, HC240), before and after thermal treatment and cycles

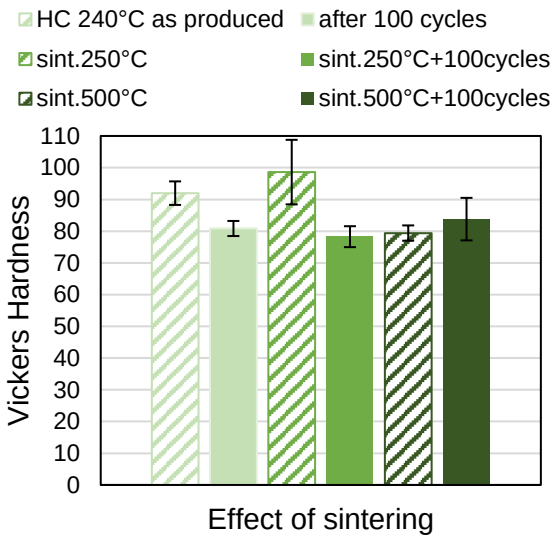

Figure 13. Vickers hardness values for sample produced by HC240 and possibly sintered at 250°C and 500°C, before and after thermal treatment and cycle

4. Discussion

As far as the microstructure is concerned, also in the case of hot compression, the effect of Sn-powder type is limited to the residual presence of some slightly coarser Sn particles in samples produced using the most heterogeneous Sn powder referred as 106, while most of the volume of the form-stable PCMs produced was characterized by the phase refinement and homogenization brought about by ball milling.

The results from XRD allow to state that the high pressures arisen during ball milling did not induce phase transformations of Sn from β-phase (stable at atmospheric pressure) to γ- and σ-phases, reported to be stable at pressures higher than 9.4 GPa and 45 GPa, respectively [23]. Moreover, the presence of other elements as impurities did not induce the formation of other phases, thus thermal and mechanical behaviour of the material can be ascribed to the microstructure of the Al-Sn alloy only. The different intensity of low-angle peaks in XRD pattern (Figure 9) is attributed to a texture effect due to the powder metallurgy process. As a matter of fact, this production process does not induce a preferential orientation of grains, therefore peaks in XRD patterns can change in intensity from sample to sample, especially if produced with different processes. In more detail, first,

mixing through ball milling caused cracking and random deformation of powder particles due to ball compression. Then, the two compression conditions could have had different effects. In hot compression at 220°C (i.e. below Sn melting temperature), the sample is compacted without melting of Sn, therefore the two phases are subjected to plastic deformation only. On the other hand, Sn melts during hot compression at 240°C and it is possible that at least coarse Sn particles solidify according to preferential directions, as observed by Ma et al. in Sn-Ag-Cu solders [24].

Considering Sn whiskers, they usually appear randomly in electronic components made of metals like Sn, Zn and Cd, causing short circuits when they become long enough [25]. According to Chason et al. [25], they are probably due to residual stresses in the metallic layer, but up to now their occurrence is not predictable and a general effective approach to suppress their formation is still necessary. In the case of ball-milled PCMs, the production process can easily cause residual stresses in the material, especially in samples compressed below Sn melting temperature and in non-sintered samples. They can cause Sn losses, if they detach or if they melt, nevertheless the amount of Sn which could be removed by this process is limited to that located very close to surface.

Compaction of ball-milled powders just below or above the melting temperature of Sn and the very close eutectic horizontal line caused a slight change in microstructure as well as in thermal response. With reference to phase diagram in Figure 1, it can be suggested that during hot compression at 240°C the external part of coarse Sn particles and part of the finer ones interact with Al to reach equilibrium composition and, during solidification, transforms in a fine Al+Sn eutectic structure (99.45 mass% Sn [26]) at the boundary of Sn particle. The presence of a phase with eutectic composition could be the cause of the undefined boundaries between Al and Sn particles. However, this feature is observed also in the samples compressed at 220°C, i.e. below eutectic temperature, also before thermal cycles simulating service. A possible explanation could be the fact that during hot

compression the alloy is subjected to high pressures, which can change the equilibrium conditions. A concurrent increase of temperature inside the die could have occurred during compaction, leading the material to the reaction temperature.

Eutectic structure is characterized by melting enthalpy of (60.84 J/g [27]), slightly higher than that of pure tin (59.58 J/g [12]). The presence of eutectic structure is not sufficient to justify the measured enthalpy of samples HC220 and HC240, slightly higher than the ones that can be calculated for Al-40Sn mass%, i.e. 23,6 J/g, and this suggest a local enrichment in Sn of the investigated DSC samples. On the other hand, the reduction of measured enthalpy after simulated service is attributed to Sn losses due to leakage during thermal cycles or sintering. In addition, sub-micrometric particles could have a latent heat significantly lower than the value for bulk material, as demonstrated by Jiang et al. [28]. Therefore, since the presence of the fine microstructure with sub-nanometric particles increases with thermal cycle and coarse Sn particles reduce simultaneously, it is possible that small particles contribute to latent heat reduction. However, this explanation has still to be explored in details and strategies to do this are under consideration.

The DSC analyses revealed a specific thermal response of the ball milled Al-Sn alloys that could be interesting for the use of FS-PCM in specific TES components. This response was not observed in simple materials with the same chemical composition produced by compaction of simple mixed powders [16]. As a matter of fact, due to the nanometric size of Sn particles, solidification is completed at lower temperatures, i.e. undercooling occurs. The transition toward lower and broader solidification peaks is more evident for the hot compacted samples cycled to simulate service. The Sn solidification in nanometric particles trapped inside the material and a corresponding undercooling during solidification is more evident in samples sintered at 500°C. The changes induced in the release of thermal energy during solidification are an interesting feature from the perspective use of the PCM for thermal management. As a matter of fact, specific components could benefit

from a fast heat storage at relatively high temperature and by its slower energy release over a relatively wide temperature range.

The distribution of Sn particles has also another effect, the possibility to prevent leakage of the active phase when it is molten. This fact has been demonstrated by the macroscopic absence of leakage from sintered samples and it is responsible for the melting/solidification enthalpy of the PCMs sintered at 500°C relatively stable over cycles simulating service. Moreover, the values obtained for Vickers hardness are in the same range as in other ball-milled Al-Sn alloys, i.e. about 80-90 HV, which are higher than the values for cast Al-Sn alloys, about 30 HV [18], and simple-mixed PCMs, about 30-40 HV [16].

As a result, among the investigated samples, the most promising Al-Sn form-stable PCMs are those produced by ball-milled powders sintered at 500°C with relatively stable microstructures, energy storage/release, hardness and negligible leakage.

5. Conclusions

1. Al-40Sn mass% samples produced by hot compression at 220 and 240°C of ball-milled Al-Sn mixed powders show minor effects of the initial size distribution of Sn powders.
2. Hot compressed specimens were characterized by fine microstructural features and by the presence of only pure Al and pure β-Sn phase. A phase with almost eutectic composition starts forming during the hot compression. Microstructural features become finer both after sintering processes at 250°C and 500°C and/or after simulated service by means of 100 cycles between 175 and 285°C.
3. In all the investigated conditions, the material hardness ranged approximately between 80 and 100 HV and the volumetric porosity was less than 4%. The material hardness, related to fine microstructural features, is almost twice that of alloys with the same nominal compositions but coarser structures, produced by compacting

and sintering under the same conditions simple mixed Al and Sn powders, previously investigated by the research group.

4. The thermal response of the Al-40Sn mass% FS-PCM was characterized by close melting/solidification enthalpies, ranging between 20 and 40 J/g. The highest values, those of samples hot compressed below the melting temperature of pure Sn, were also the less stable, due to microstructural changes and possible Sn losses. Samples hot compressed at 240°C displayed a better thermal stability. Among them, those further sintered at 500°C were the most stable both from a thermal and mechanical point of view. During active-phase transition, the fine microstructure of these FS-PCMs is able to prevent Sn leakage and to have suitable thermal response, consisting in a relatively fast thermal storage and a slower heat release.

Acknowledgements

The authors would like to thank for their help in characterization tests Paola Bassani, Enrico Bassani and Maxime Perrin.

This work was supported by the Italian Ministry for Education, University and Research through the project Department of Excellence LIS4.0 (Integrated Laboratory for Lightweight e Smart Structures).

Author contributions

Chiara Confalonieri: Investigation, Formal analysis, Writing – Original Draft, Writing – Review and Editing. Aldo Tommaso Grimaldi: Investigation, Writing – Review and Editing. Elisabetta Gariboldi: Conceptualization, Methodology, Investigation, Writing – Review and Editing.

Declarations of interest

None.

Data availability

The raw data required to reproduce these findings cannot be shared at this time as the data also forms part of an ongoing study. The processed data required to reproduce these findings cannot be shared at this time as the data also forms part of an ongoing study.

References

[1] M. Kuta, D. Matuszewska, T.M. Wójcik, The role of phase change materials for the sustainable energy, E3S Web Conf. 10 (2016) 68. doi:10.1051/e3sconf/20161000068.

[2] T. Fiedler, A.J. Rawson, H. Sugo, E. Kisi, Thermal capacitors made from Miscibility Gap Alloys (MGAs), in: WIT Trans. Ecol. Environ., WIT Press, 2014: pp. 479–486. doi:10.2495/ESUS140411.

[3] N. Navarrete, A. Gimeno-Furio, R. Mondragon, L. Hernandez, L. Cabedo, E. Cordoncillo, J.E. Julia, Nanofluid based on self-nanoencapsulated metal/metal alloys phase change materials with tuneable crystallisation temperature, Sci. Rep. 7 (2017) 17580. doi:10.1038/s41598-017-17841-w.

[4] S. Reed, H. Sugo, E. Kisi, High temperature thermal storage materials with high energy density and conductivity, Sol. Energy. 163 (2018) 307–314. doi:10.1016/J.SOLENER.2018.02.005.

[5] H. Nazir, M. Batool, F.J. Bolivar Osorio, M. Isaza-Ruiz, X. Xu, K. Vignarooban, P. Phelan, Inamuddin, A.M. Kannan, Recent developments in phase change materials for energy storage applications: A review, Int. J. Heat Mass Transf. (2019).

doi:10.1016/j.ijheatmasstransfer.2018.09.126.

[6] J.Q. Sun, R.Y. Zhang, Z.P. Liu, G.H. Lu, Thermal reliability test of Al–34%Mg–6%Zn alloy as latent heat storage material and corrosion of metal with respect to thermal cycling, Energy Convers. Manag. 48 (2007) 619–624. doi:10.1016/J.ENCONMAN.2006.05.017.

[7] G. Wei, G. Wang, C. Xu, X. Ju, L. Xing, X. Du, Y. Yang, Selection principles and thermophysical properties of high temperature phase change materials for thermal energy storage: A review, Renew. Sustain. Energy Rev. 81 (2018) 1771–1786. doi:10.1016/J.RSER.2017.05.271.

[8] S.A. Mohamed, F.A. Al-Sulaiman, N.I. Ibrahim, M.H. Zahir, A. Al-Ahmed, R. Saidur, B.S. Yılbaş, A.Z. Sahin, A review on current status and challenges of inorganic phase change materials for thermal energy storage systems, Renew. Sustain. Energy Rev. 70 (2017) 1072–1089. doi:10.1016/J.RSER.2016.12.012.

[9] C. Zhou, S. Wu, Medium- and high-temperature latent heat thermal energy storage: Material database, system review, and corrosivity assessment, Int. J. Energy Res. 43 (2019) 621–661. doi:10.1002/er.4216.

[10] J. Paris, M. Falardeau, C. Villeneuve, Thermal Storage by Latent Heat: A Viable Option for Energy Conservation in Buildings, Energy Sources. 15 (1993) 85–93. doi:10.1080/00908319308909014.

[11] W. Su, J. Darkwa, G. Kokogiannakis, Review of solid–liquid phase change materials and their encapsulation technologies, Renew. Sustain. Energy Rev. 48 (2015) 373–391. doi:https://doi.org/10.1016/j.rser.2015.04.044.

[12] W. Shackelford, James F., Alexander, ed., CRC Materials Science and Engineering Handbook, 3rd ed., CRC Press, Boca Raton, 2001.

doi:https://doi.org/10.1201/9781420038408.

[13] K. Pielichowska, K. Pielichowski, Phase change materials for thermal energy storage, Prog. Mater. Sci. 65 (2014) 67–123. doi:10.1016/J.PMATSCI.2014.03.005.

[14] H. Sugo, E. Kisi, D. Cuskelly, Miscibility gap alloys with inverse microstructures and high thermal conductivity for high energy density thermal storage applications, Appl. Therm. Eng. 51 (2013) 1345–1350. doi:10.1016/J.APPLTHERMALENG.2012.11.029.

[15] X. Liu, M.Q. Zeng, Y. Ma, M. Zhu, Melting behavior and the correlation of Sn distribution on hardness in a nanostructured Al–Sn alloy, Mater. Sci. Eng. A. 506 (2009) 1–7. doi:10.1016/J.MSEA.2008.12.054.

[16] E. Gariboldi, M. Perrin, Metallic Composites as Form-Stable Phase Change Alloys, in: THERMEC 2018, Trans Tech Publications, 2019: pp. 1966–1971. doi:10.4028/www.scientific.net/MSF.941.1966.

[17] N.I. Noskova, N.F. Vil'danova, Y.I. Filippov, R. V Churbaev, I.A. Pereturina, L.G. Korshunov, A. V Korznikov, Preparation, deformation, and failure of functional Al-Sn and Al-Sn-Pb nanocrystalline alloys, Phys. Met. Metallogr. 102 (2006) 646–651. doi:10.1134/S0031918X06120131.

[18] X. Liu, M.Q. Zeng, Y. Ma, M. Zhu, Promoting the high load-carrying capability of Al–20wt%Sn bearing alloys through creating nanocomposite structure by mechanical alloying, Wear. 294–295 (2012) 387–394. doi:10.1016/j.wear.2012.07.021.

[19] C. Suryanarayana, Mechanical alloying and milling, Prog. Mater. Sci. 46 (2001) 1–184. doi:https://doi.org/10.1016/S0079-6425(99)00010-9.

[20] C. Confalonieri, Z. Li, E. Gariboldi, Metallic Form-Stable Phase Change Materials for Thermal Energy Storage and Management: general features and effect of

manufacturing process on thermal response and stability, La Metall. Ital. - Int. J. Ital. Assoc. Metall. 7/8 (2019) 12–20.

[21] E. Underwood, The Mathematical Foundations of Quantitative Stereology, in: G. Pellissier, S. Purdy (Eds.), Stereol. Quant. Metallogr., ASTM International, West Conshohocken, PA, 1972: pp. 3–38. doi:10.1520/STP36841S.

[22] W.S. Rasband, ImageJ, (2018). https://imagej.net/Welcome.

[23] W. Steurer, Crystal Structures of the Elements, Encycl. Mater. Sci. Technol. (2001) 1880–1897. doi:10.1016/B0-08-043152-6/00344-2.

[24] Z.L. Ma, H. Shang, A.A. Daszki, S.A. Belyakov, C.M. Gourlay, Mechanisms of beta-Sn nucleation and microstructure evolution in Sn-Ag-Cu solders containing titanium, J. Alloys Compd. 777 (2019) 1357–1366. doi:https://doi.org/10.1016/j.jallcom.2018.11.097.

[25] E. Chason, F. Pei, N. Jain, A. Hitt, Studying the Effect of Grain Size on Whisker Nucleation and Growth Kinetics Using Thermal Strain, J. Electron. Mater. 48 (2019) 17–24. doi:10.1007/s11664-018-6594-x.

[26] A.J. McAlister, D.J. Kahan, The Al−Sn (Aluminum-Tin) System, Bull. Alloy Phase Diagrams. 4 (1983) 410–414. doi:10.1007/BF02868095.

[27] B. Predel, Al-Sn (Aluminum-Tin): Datasheet from Landolt-Börnstein - Group IV Physical Chemistry · Volume 5A: “Ac-Au – Au-Zr” in SpringerMaterials, 5A (1991). doi:10.1007/10000866_144.

[28] B. Yang, Y. Gao, C. Zou, Q. Zhai, E. Zhuravlev, C. Schick, Size-dependent undercooling of pure Sn by single particle DSC measurements, Chinese Sci. Bull. 55 (2010) 2063–2065. doi:10.1007/s11434-010-3041-7.